Proceedings of the ASME 2010 3rd Joint US-European Fluids Engineering Summer Meeting and 8th International Conference on Nanochannels, Microchannels, and Minichannels
FEDSM-ICNMM2010
August 1-5, 2010, Montreal, Canada

FEDSM-ICNMM2010-30020

MEMS-BASED MICROFLUIDIC DEVICES

Z. Gao
Eastman Kodak Company
Rochester, NY USA

K. Ng
Eastman Kodak Company
Rochester, NY USA

E. Furlani
Eastman Kodak Company
Rochester, NY USA

J. Chwalek
Eastman Kodak Company
Rochester, NY USA

G. Hawkins
Eastman Kodak Company
(retired)
Rochester, NY USA

ABSTRACT

Micro-Electro-Mechanical Systems (MEMS) technology can be integrated with microfluidic functionality to enable the generation of microdrops with unprecedented throughput and precise control of drop volume, speed, and placement. The most prominent examples of microdrop generators are in the field of inkjet printing where printheads with thousands of nozzles produce steady streams of microdrops at kilohertz repetition rates. In this paper, we discuss a proposed MEMS-based microfluidic drop generator that operates on the basis of a thermally induced Marangoni effect. We describe the physics of droplet generation and discuss operating performance relative to the fluid rheology, thermal modulation, and wavelength dependencies.

INTRODUCTION

Microfluidics deals with the behavior, precise control, and manipulation of fluids that are geometrically constrained to a small, typically submillimeter scale. It is a multidisciplinary field that intersects engineering, physics, chemistry, microtechnology, and biotechnology, with practical applications that involve systems in which such small volumes of fluids are used. Microfluidics emerged in the beginning of the 1980s and is used in the development of inkjet printheads, DNA chips, lab-on-a-chip technology, micro propulsion, and micro thermal technologies. Over the past few years, microfluidics devices have enjoyed success in certain niche applications, notably inkjet printers and lab-on-a-chip assays.

Advances in microfluidics technology are revolutionizing molecular biology procedures for enzymatic analysis (e.g., glucose and lactate assays), DNA analysis (e.g., polymerase chain reaction and high-throughput sequencing), and proteomics. The basic idea of microfluidic biochips is to integrate assay operations such as detection, as well as sample pre-treatment and sample preparation on one chip. An emerging application area for biochips is clinical pathology, especially the immediate point-of-care diagnosis of diseases. In addition, microfluidics-based devices, capable of continuous sampling and real-time testing of air/water samples for biochemical toxins and other dangerous pathogens, can serve as an always-on "bio-smoke alarm" for early warning.

Inkjet printing for consumer applications has revolutionized desktop printing of documents, including high-quality color images. The two currently commercialized printhead technologies, thermal and piezo drop-on-demand (DOD) technologies, contribute substantially to the revenues attributed to MEMS devices. These technologies have been slow to penetrate commercial applications because the printing speed of consumer devices is far less than that typically associated with technologies such as offset lithography. Of course, the speed of offset printing derives from the fact that identical images are produced without variable data content. The desirability to print variable data at the speed and cost of offset printing has long been recognized but not yet achieved.

We believe that the continuous inkjet (CIJ) technology proposed and described here offers a practical path for such offset class digital printing. This new CIJ technology benefits from the convergence of new principles of device operation, the availability of integrated electronic/fluidic device manufacturing, as well as new developments in ink and media formulations.

Figure 1 illustrates schematically a new type of silicon-based CIJ printhead based on thermally stimulated drop formation. Ink in the reservoir is pressurized and jets through the nozzles in the form of fluid columns that propagate and eventually break up into drops. Figure 2 shows a cross-section of a CIJ device of the thermal stimulation type, which is made by integrated complementary metal-oxide semiconductor (CMOS)-MEMS processing using deep reactive ion etching to form the ink reservoirs as channels through the silicon wafer. The nozzle bores are etched through all of the various dielectric layers of the CMOS process and are typically 10 µm in diameter and located on 20–40 µm centers. The choice of silicon as a material technology is an important one, both because silicon-based materials have historical precedence for their compatibility with liquid inks, and because the ability to integrate electronic logic for nozzle addressing greatly simplifies the already complex fluidic packaging of devices with thousands of nozzles.

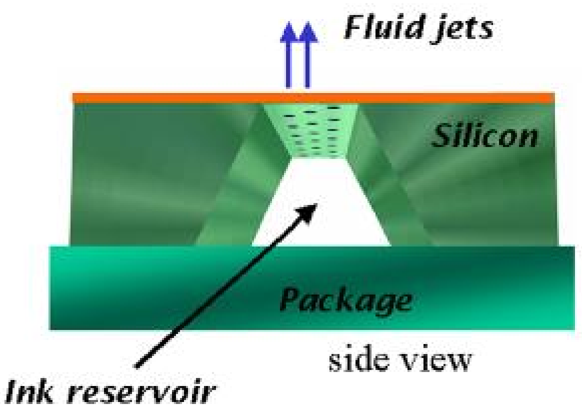

Figure 1. A schematic view of a microfluidic inkjet printhead that is based on thermally induced drop generation from an array of continuously jetted fluid streams.

In contrast to DOD printheads, the energy supplied to eject fluids in CIJ technology is not local to the nozzles. For example, the reservoir in Figure 1 contains fluid pressurized by a pump external to the printhead. Due to the strength of silicon materials and the fact that the drop generation energy does not have to be supplied by microactuators integrated with each nozzle, it is possible to eject a very wide variety of fluids by continuously maintaining many atmospheres of pressure in the reservoir. Because the pressure is constant in CIJ technology, rather than being pulsed as in DOD technology, the duty cycle for fluid ejection is 100% and the velocity of the jets can be varied over a wide range, for example 10–40 m/s.

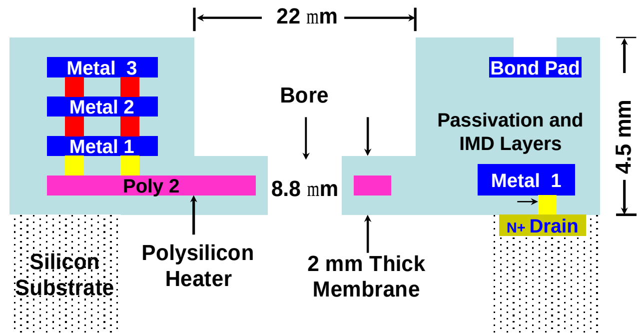

Figure 2. Cross-section of CMOS-MEMS integrated printhead.

Figure 2 is a schematic showing a cross-section of the material layers in a single CIJ nozzle. Figure 3 is a scanning electron microscope (SEM) micrograph of a nozzle bore formed in a CMOS interlayer dielectric stack and of the associated embedded heater formed in first gate polysilicon, in accordance with the schematic illustration of Figure 2. The heater ring closely surrounding the bore in Figure 3 cannot be seen on the surface of the membrane through which the bore is formed due to the planarity of the fabrication process. The rectangular structures in Figure 3 are metal traces connecting the CMOS driver to the heater. The use of very-large-scale integration (VLSI) processing results in very precise geometries for the jet exit orifice and for the heater. This precision is important to ensure accurate jet directionality. The membrane surrounding the 10 µm diameter nozzle bore is less than 2 µm in thickness.

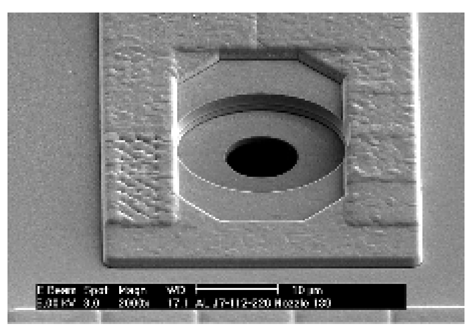

Figure 3. Silicon nozzle; the bore diameter is about 8 µm. The 1 µm width thin-film heater is buried in the dielectric layers adjacent the opening.

PHYSICS OF DROP FORMATION AND CONTROL

The capillary instability of liquid jets has been the subject of numerous studies since the19th century when Lord Rayleigh considered the breakup of an inviscid cylindrical jet into drops [1, 2]. However, the subject has been far from exhausted after more than several centuries of scientific research, which in fact has gained considerable momentum in recently years. This is due partially to the fact that modern developments in the design and utilization of microfluidic devices for fluid transport have found many applications such as drug design and diagnostic devices in biomedicine and microdrop generators for image printing. Furthermore, the new development of nonlinear dynamics of the droplet has created a new paradigm of scaling and jet breakup that opened a new approach to this classic phenomenon. Currently, there is a considerable amount of literature available on Newtonian liquid jet instability. Some of the related references are reviewed in Gao [3]. However, the situation is more difficult for non-Newtonian jets caused by the complex nature of the constitutive behavior of such a liquid. Axisymmetric instability of non-Newtonian jets was studied by Sterling and Sleicher [4]; Lin and Lian [5]; Lin and Ibrahim [6]; Brenn et al. [7]; and Liu and Liu [8]. Liu and Liu [8] extended the work on Newtonian jets done by Li [9] to investigate the mechanisms of temporal instability of viscoelastic liquid jets with both axisymmetric and asymmetric disturbances, and to explore the differences between the instabilities of axisymmetric and asymmetric disturbances, concentrating on the wind-induced regime. Yildirim and Basaran [10] studied the deformation and breakup of bridges of Newtonian and non-Newtonian fluids held captive between two disks that are separated from one another at a constant speed. Nevertheless, relatively few authors have studied jet instability caused by spatial variations of surface tension, despite the practical relevance of this phenomenon [3, 12-13].

To modulate a jet of the inkjet printhead shown in Figures 1-3, a periodic voltage is applied to the heater, which causes a periodic diffusion of thermal energy from the heater into the fluid near the orifice (Figure 4). Thus, the temperature of fluid, and hence the temperature-dependent fluid properties, density, viscosity, and surface tension, are modulated near the orifice. The dominant cause of jet instability is the modulation of surface tension. To first order, the temperature dependence of s is given by $s(T) = s_0 - b(T - T_0)$, where $s(T)$ and s_0 are the surface tension at temperatures T and T_0, respectively. The pulsed heating modulates s at a wavelength λ = v_0τ, where v_0 is the jet velocity and τ is the period of the heat pulse as shown in Figure 4. The down-stream advection of thermal energy gives rise to a spatial variation (gradient) of surface tension along the jet. This produces a shear stress at the free-surface, which is balanced by inertial forces in the fluid, thereby inducing a Marangoni flow toward regions of higher surface tension (from warmer regions toward cooler regions). This causes a deformation of the free-surface (slight necking in the warmer regions and ballooning in the cooler regions) that ultimately leads to instability and drop formation [3, 12-13]. The drop volume can be adjusted on demand by varying τ, i.e., $V_{drop} = p r_0^2 v_o \tau$. Thus, longer pulses produce larger drops, shorter pulses produce smaller drops, and different sized drops can be produced from each orifice as desired.

The governing equations for a jet of incompressible fluid, Figure 4, are the continuity equation and the momentum equation (ignoring gravity)

$$\nabla \cdot \boldsymbol{V} = 0 \tag{1}$$

$$r\left(\frac{\partial}{\partial t} + \boldsymbol{V} \cdot \nabla\right)\boldsymbol{V} = \nabla \cdot \boldsymbol{T} \tag{2}$$

where t is time, $\boldsymbol{V}$ is the jet velocity vector, $\boldsymbol{T}$ is the total stress tensor given as $\boldsymbol{T} = -p\boldsymbol{I} + t$, where p is the pressure of the liquid, t is the stress tensor of the liquid, and $\boldsymbol{I}$ is the unit tensor. Also, $\boldsymbol{V} = (u, v)$ is the velocity, where u and v denote the radial and axial velocities, respectively. The stress tensor, which is given by $\boldsymbol{T} = -p\boldsymbol{I} + m(\dot{g})[\nabla\boldsymbol{V} + (\nabla\boldsymbol{V})^T]$, where $m(\dot{g})$ is the apparent viscosity function. The Carreau-Yasuda model describing the deformation rate-dependent viscosity function is

$$m(\dot{g}) = (m_0 - m_\infty)\left(1 + \left|l\dot{g}\right|^a\right)^{\frac{n-1}{a}} + m_\infty \tag{3}$$

where

$$\dot{g} = \left[2\left(\frac{\partial u}{\partial r}\right)^2 + \left(\frac{\partial u}{\partial z} + \frac{\partial v}{\partial r}\right)^2 + 2\left(\frac{\partial v}{\partial z}\right)^2\right]^{1/2} \tag{4}$$

is the second invariant of rate-of-deformation tensor, and n is a power law exponent.

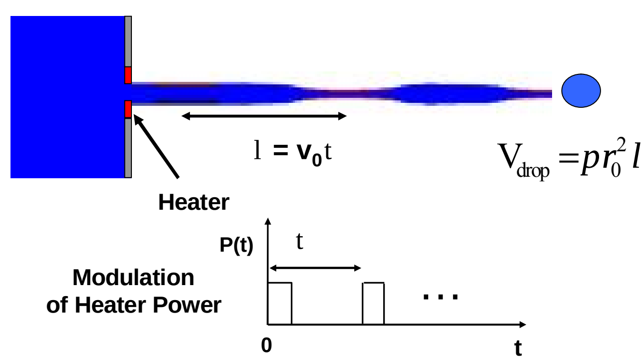

Figure 4. Illustration showing a single nozzle with an integrated heater at the orifice, and a thermal modulation pulse used to induce Marangoni instability and drop formation.

The Carreau-Yasuda model is one of the models used for describing the viscosity of a non-Newtonian fluid. Typically, based on the number of parameters, this is classified into three, four, and five parameter types, wherein the parameters m_∞, l, and n are material coefficients, where, m_∞ is the limiting viscosity at high shear stress, l is a time constant calculated from the reciprocal of the strain rate at which the zero strain rate component and the power-law component of the flow curve intersect, and n is called Thixotropic index. The Thixotropic index is a ratio of a material's viscosity at two different speeds, generally different by a factor of ten. This index indicates the material's ability to hold its shape. The three-parameter model is called the Bird-Carreau model and the five-parameter model is the Carreau-Yasuda model. The power law model represents a deformation-rate-thinning fluid when $n < 1$, a deformation rate- thickening fluid when $n > 1$, and a Newtonian fluid when $n = 1$. The Carreau-Yasuda model describes pseudoplastic flow with asymptotic viscosities at zero (m_0) and infinite (m_∞) shear rates, and with no yield stress. The parameter λ is a constant with units of time, where $1/\lambda$ is the critical shear rate at which viscosity begins to decrease. The power law slope is $(n - 1)$ and the parameter α represents the width of the transition region between m_0 and the power law region. If m_0 and m_∞ are not known independently from experiment, these quantities may be treated as additional adjustable parameters.

Equations (1) and (2) are solved subject to stress balance condition and kinematic condition. The traction boundary condition for normal stress and shear stress can be written as, respectively,

$$\left(\vec{n}\cdot\boldsymbol{T}\right)\cdot\vec{n} = -2Hs \tag{5}$$

$$\left(\boldsymbol{T}\cdot\vec{n}\right)\cdot\vec{t} = \frac{1}{\sqrt{1+h'^2}}\frac{\partial s}{\partial z} \tag{6}$$

where

$$H = \frac{1}{2}\left(\frac{1}{h\sqrt{1+h'^2}} - \frac{h''}{\sqrt{(1+h'^2)^3}}\right) \tag{7}$$

$$\vec{n} = \frac{1}{\sqrt{1+h'^2}}\vec{r} - \frac{h'}{\sqrt{1+h'^2}}\vec{z} \tag{8}$$

$$\vec{t} = \frac{h'}{\sqrt{1+h'^2}}\vec{r} + \frac{1}{\sqrt{1+h'^2}}\vec{z} \tag{9}$$

In these equations, $h(z, t)$ defines the radial position of the jet's free surface, and $h' = \frac{\partial h}{\partial z}$, and $s = s(z,t)$ is the surface tension, $\frac{\partial s}{\partial z} = \frac{\partial s(z,t)}{\partial z}$.

For slender microjets, Equations (1) and (2) can be simplified using a perturbation expansion in r for the unknown variables h, T and n, and retaining the lowest order terms [5]. This leads to the following 1-D slender jet equations:

$$\frac{\partial v_0}{\partial t} + v_0\frac{\partial v_0}{\partial z} = -\frac{1}{r}\frac{\partial}{\partial z}(2s\,H) + \frac{2}{r\,h}\frac{\partial s}{\partial z} + \frac{3}{r\,h^2}\frac{\partial}{\partial z}\left(h^2 m(z,t)\frac{\partial v_0}{\partial z}\right) \tag{10}$$

$$\frac{\partial h}{\partial t} + v_O\frac{\partial h}{\partial z} = -\frac{1}{2}h\frac{\partial v_0}{\partial z} \tag{11}$$

When we restrict to an analysis the purely temporal instability behavior of the jet (i.e., we do not consider traveling waves on the jet) and introduce a new variable $h = z - V_0 t$, Equations (10) and (11) can be considered as two Partial Differential Equation (PDE) for variables h and t, subjected to periodic boundary conditions and zero initial conditions

$$d(h, t=0) = 0, \text{ and } \frac{\partial d}{\partial t}(h, t=0) = 0 \text{ for all } h.$$

where V_0 is the unperturbed velocity of the jet.

When a constitutive law for viscosity $m(h,t)$ is specified, Equations (10) and (11) can be solved to determine the jet profile, h, as a function of time. The deformation rate defined in Equation (4) can be further simplified as keeping only the leading term in r,

$$\dot{g} = [2(\frac{\partial v_r}{\partial r})^2 + 2(\frac{v_r}{r})^2 + (\frac{\partial v_r}{\partial z} + \frac{\partial v_z}{\partial r})^2 + 2(\frac{\partial v_z}{\partial z})^2]^{1/2}$$

$$= \sqrt{3(\frac{\partial v}{\partial z})^2} = \sqrt{3}\left|\frac{\partial v}{\partial z}\right| = 2\sqrt{3}\left|\frac{\partial d}{\partial t}\right|$$

Therefore, for the Carreau-Yasuda model shown in Equation (3), we have

$$
\begin{aligned}
m(h,t) &= (m_0 - m_\infty)[1 + \left|t\dot{g}\right|^a]^{\frac{n-1}{a}} + m_\infty \\
&= (m_0 - m_\infty)[1 + \left|2\sqrt{3}t\,\frac{\partial d}{\partial t}\right|^a]^{\frac{n-1}{a}} + m_\infty
\end{aligned}
\qquad (12)
$$

The jet breakup is driven by the gradient of surface tension $s_1(h)$. The surface tension can be modulated by thermal simulation to the surface of the jet as it exits the orifice, and can take different forms [12-13]. One way to simplify the mathematics involved is to select cosine wave, i.e.,

$$
s_1(h) = -\frac{\Delta s}{2}[1 + Cos(\frac{hk}{r_0})]. \qquad (13)
$$

In many applications, such as inkjet applications shown in Figure 4, the cosine wave may not be optimal. In such a case, the temperature profile, as well as the surface tension of the fluid, is represented as a function

$$
\begin{aligned}
s_1(h) &= -\Delta s\,(1 - e^{-ht_1/l}) && h < h_1 \\
s_1(h) &= -\Delta s\,(1 - e^{-ht_1/l})e^{-(h-h_1)t_2/l} && h \geq h_1
\end{aligned}
\qquad (14)
$$

where t_1 and t_2 are parameters that indicate how fast the temperature reaches its plateau level, and how fast it decays from the plateau level to zero, respectively. This ratio of actuation pulse time to the total period (actuation pulse time plus delay time) is known within the art as duty cycle. Generally, a high frequency of activation of heater results in small-volume droplets, while a low frequency of activation of heater results in large volume droplets.

RESULTS AND DISCUSSION

We demonstrate the model via application to a microjet of poly-Nisopropylacrylamide (poly-NIPAM) microgel solution. The properties are ρ = 1000 kgm^{-3}, r_0 = 5 μm, v_0 = 10 ms^{-1}, s_0 = 0.073 N m^{-1}. Other parameters depend on the concentration of the microgel.

The Partial Differential Equation (PDE) for the perturbation of the radius of the microjet, Equations (10) and (11), with periodic boundary conditions and zero initial conditions, is solved by the method of lines [11]. The initial condition for the system of Ordinary Differential Equation (ODE) is y = 0. We implement this numerical scheme in MATLAB and use its ODE solver ode15s to solve the system of ODE.

Figure 5 shows the breakup time in 10^(-5) seconds of a Newtonian fluid due to the cosine modulation, Equation (13) and exponential modulation, Equation (14), respectively, for three values of t_1 and t_2. The parameters are m_0 = 0.01 N sm^{-2}, h_1 = 30%λ, where λ = 2πr/k (r – radius of the jet, k – wave number). The parameter $t = t_1 = t_2$ represents the rate of surface temperature increase and decrease of the jet. A higher t means a fast ramping up of the temperature when the heater is turned on, while a higher t means a fast ramping down of the temperature when the heater is turned off. It is shown in Figure 5 that when the value of t is equal to 1, the exponential modulation produces a lower breakup time than that of the cosine modulation, only when at small wave number k (k < 0.45). When the wave number k is larger than 0.45, the exponential wave form gives a slightly higher breakup time in comparison with that from the cosine modulation. The two modulations have the same area under the curves to ensure that they have the same thermal modulation power. When the value of t is increased from 1 to 10 and to 20, Figure 5, the curve for the exponential modulation moves down slightly. Although the breakup time for t equal to 10 and 20 are always lower for the exponential modulation regardless the wave number, the difference between the two curves (exponential and cosine) are only substantial at the wave number lower than 0.45. When the value of t is equal to 20, the exponential modulation is very close to a square modulation with sharp increase and decrease of the surface tension. It is believed that in comparison with the cosine wave, square wave is more effective at breaking up a jet since the square wave focuses its thermal energy to a smaller portion of the jet. However, it is shown from Figure 5 that this is true only for a smaller value wave number. The results for non-Newtonian fluid represented by the Carreau-Yasuda model are shown in Figure 6. Again the effect of the exponential modulation is significant only when the wave number is small.

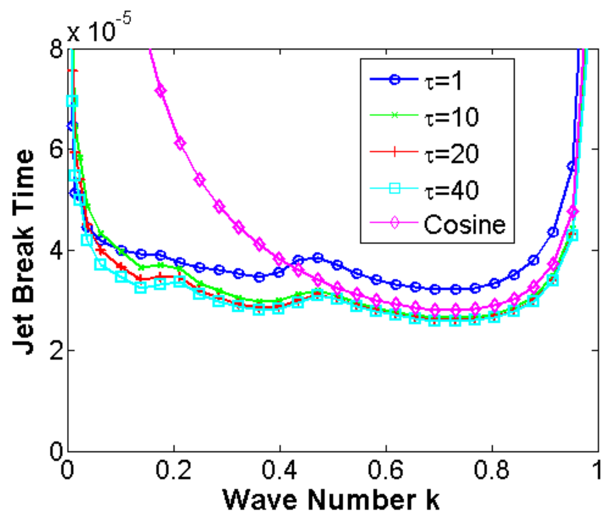

Figure 5. The breakup time in 10^(-5) seconds of a Newtonian fluid due to the cosine modulation and exponential modulation, respectively,. The parameters are m_0 = 0.001 N sm^{-2}, h_1 = 30%λ, where λ = 2πr/k (r – radius of the jet, k – wave number).

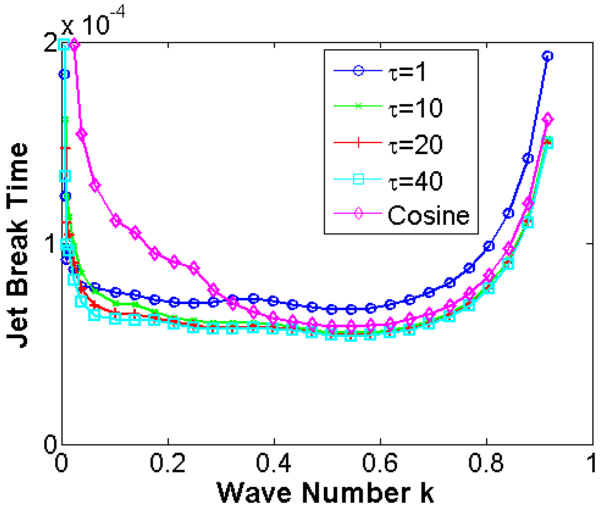

Figure 6. The breakup time in 10^(-4) seconds of a Carreau fluid due to the cosine modulation, Eqn. (28) and exponential modulation, Eqn. (29), respectively,. The parameters are n = 0.64, m_0 = 0.026 N sm^{-2}, m_∞ = 0.008 N sm^{-2}, l = 0.2 s^{-1}, α = 1.4. The surface tension and surface tension variation are s_0 = 0.073 N m^{-1} and Δs =1% s_0, respectively.

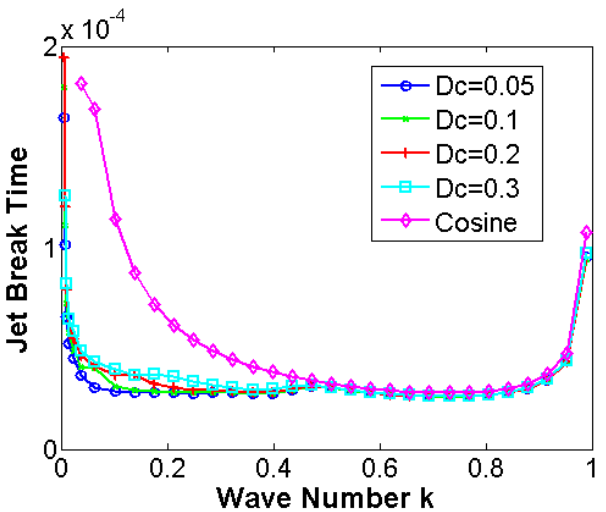

Figure 7. The comparisons of breakup time in 10^(-4) seconds for Carreau liquids under sinusoidal modulation and exponential modulation with various values of duty cycle. The coefficients t_1 and t_2 of the exponential modulation have the value of 20.

The comparisons of break time for Carreau liquids under sinusoidal modulation and exponential modulation with various values of duty cycle are shown in Figure 7. The coefficient $t = t_1 = t_2$ of the exponential modulation has the value of 20. Other parameters are l = 0.2 s^{-1}, α = 1.4. The surface tension and surface tension variation are s_0 = 0.073 N m^{-1} and Δs =1% s_0, respectively.

REFERENCES

1. Rayleigh Lord 1878 On the Instability of Jets, *Proc. London, Math. Soc. X.*
2. Rayleigh Lord 1899 *Scientific Papers* (London: Cambridge University Press) Vol. I, p. 361.
3. Gao Z. Instability of non-Newtonian jets with a surface tension gradient. *J Phys A: Math Theor* 2009;42.
4. Sterling A M and Sleicher C A 1975 The instability of capillary jets J. Fluid Mech. 68 477–495.
5. Lin S P and Lian Z W 1990 Mechanism of the breakup of liquid jets AIAA J. 28 120–126.
6. Lin S P and Ibrahim E A 1990 Instability of a viscous liquid jet surrounded by a viscous gas in a vertical pipe J. Fluid Mech. 218 641–658.
7. Brenn G, Liu Z and Durst F 2000 Linear analysis of the temporal instability of axisymmetrical non-Newtonian liquid jets Intl. J. Multiphase Flow 26 1621–1644.
8. Liu Z and Liu Z 2006 Linear analysis of three-dimensional instability of non-Newtonian liquid jets J. Fluid Mech. 559 451–459.
9. Li X 1995 Mechanism of atomization of a liquid jet Atomization Sprays 5 89–105.
10. Yildirim O E and Basaran O 2001 Deformation and breakup of stretching bridges of Newtonian and shear-thinning liquids: comparison of one- and two-dimensional models Chemical Engineering science 56, 211-233.
11. Byrne G D and Schiesser W E 1992 Recent Developments in Numerical Methods and Software for ODEs/DAEs/PDEs, Published by World Scientific, pp.208.
12. Furlani E P 2005 Temporal instability of viscous liquid microjets with spatially varying surface tension *J. Phys. A: Math. Gen*. **38** 263–276.
13. Gao Z and Ng K. Temporal analysis of power law liquid jets, *Computers & Fluids* **39** (2010) 820–828.